The Astrophysical Journal Letters, 973:L49 (9pp), 2024 October 1 https://doi.org/10.3847/2041-8213/ad74e2

Birth of Rapidly Spinning, Overmassive Black Holes in the Early Universe

Kohei Inayoshi[1] and Kohei Ichikawa[2,3]
[1] Kavli Institute for Astronomy and Astrophysics, Peking University, Beijing 100871, People's Republic of China; inayoshi@pku.edu.cn
[2] Global Center for Science and Engineering, Faculty of Science and Engineering, Waseda University, 3-4-1, Okubo, Shinjuku, Tokyo 169-8555, Japan
[3] Department of Physics, School of Advanced Science and Engineering, Faculty of Science and Engineering, Waseda University, 3-4-1, Okubo, Shinjuku, Tokyo 169-8555, Japan
Received 2024 February 22; revised 2024 July 20; accepted 2024 August 27; published 2024 September 26

Abstract

The James Webb Space Telescope (JWST) has unveiled numerous massive black holes (BHs) in faint, broad-line active galactic nuclei (AGNs). The discovery highlights the presence of dust-reddened AGN populations, referred to as "little red dots (LRDs)," more abundant than X-ray-selected AGNs, which are less influenced by obscuration. This finding indicates that the cosmic growth rate of BHs within this population does not decrease but rather increases at higher redshifts beyond $z \sim 6$. The BH accretion rate density deduced from their luminosity function is remarkably higher than that from other AGN surveys in X-ray and infrared bands. To align the cumulative mass density accreted to BHs with the observed BH mass density at $z \simeq 4$–5, as derived from the integration of the BH mass function, the radiative efficiency must be doubled from the canonical 10% value, achieving significance beyond the $>3\sigma$ confidence level. This suggests the presence of rapid spins with 96% of the maximum limit among these BHs under the thin-disk approximation, maintained by prolonged mass accretion instead of chaotic accretion with randomly oriented inflows. Moreover, we derive an upper bound for the stellar mass of galaxies hosting these LRDs, ensuring consistency with galaxy formation in the standard cosmological model, where the host stellar mass is limited by the available baryonic reservoir. Our analysis gives a lower bound for the BH-to-galaxy mass ratio that exceeds the typical value known in the nearby universe and aligns with that for JWST-detected unobscured AGNs. Accordingly, we propose a hypothesis that the dense, dust-rich environments within LRDs facilitate the emergence of rapidly spinning and overmassive BH populations during the epoch of reionization. This scenario predicts a potential association between relativistic jets and other high-energy phenomena with overmassive BHs in the early universe.

Unified Astronomy Thesaurus concepts: Galaxy formation (595); High-redshift galaxies (734); Quasars (1319); Supermassive black holes (1663)

1. Introduction

The cosmic evolution of massive black hole (BH) populations is predominantly driven by mass accretion, powering active galactic nuclei (AGNs; e.g., D. Lynden-Bell 1969) with a certain level of merger contributions to BHs harbored in nearby massive ellipticals (e.g., S. T. McWilliams et al. 2014; A. Kulier et al. 2015). Multiwavelength observations have consistently shown that AGN activity peaks around $z \sim 2$ and declines toward higher redshifts (e.g., I. Delvecchio et al. 2014; Y. Ueda et al. 2014). The analysis of AGN activity offers insights into the radiative efficiency of accreting BHs by comparing it with the local mass density of relic BHs (A. Sotan 1982; Q. Yu & S. Tremaine 2002).

Recent observations by the James Webb Space Telescope (JWST) have revealed a new category of dust-reddened, broad-line AGNs, often referred to as "little red dots" (LRDs; J. Matthee et al. 2024). These AGNs are characterized by their compact morphology and moderate dust obscuration ($A_V \approx 3$) in the spectra (D. D. Kocevski et al. 2023; I. Labbe et al. 2023; Y. Harikane et al. 2023; G. Barro et al. 2024). Investigations into the AGN luminosity function of LRDs at $z = 4$–8 found an abundance of $\Phi \sim 10^{-5}$–$10^{-4}\,\mathrm{cMpc^{-3}\,mag^{-1}}$ in the observed UV absolute magnitude range of $-22 \lesssim M_{\rm UV} \lesssim -18$ (e.g., V. Kokorev et al. 2024), significantly exceeding those predicted by extrapolations from the unobscured AGN luminosity function in ground-based surveys (e.g., M. Niida et al. 2020). Moreover, spectroscopic analysis of LRDs, facilitating direct measurement of broad Hα emissions—a tracer of AGN activity (J. E. Greene & L. C. Ho 2005)—has led to the construction of the AGN bolometric luminosity function for LRDs. This result suggests that in contrast to expectations based on AGN surveys in the pre-JWST era, the cosmic growth rate of BHs within this AGN population does not decline but appears to increase at higher redshifts ($z > 6$).

In this Letter, compiling data from extensive high-z AGN and LRD surveys, we constrain the radiative efficiency of BHs in dominant LRD populations by comparing the observed BH mass density at $z \simeq 4$–5 to the mass accreted to BHs calculated from the BH growth rate, i.e., the Soltan–Paczyński argument at the epoch of reionization. This analysis suggests a radiative efficiency higher than the canonical 10% value and favors rapid spins of these BHs under the thin-disk approximation (e.g., I. D. Novikov & K. S. Thorne 1973; N. I. Shakura & R. A. Sunyaev 1973). Furthermore, we establish an upper limit for the stellar mass of galaxies harboring these LRDs and give a lower bound for the BH-to-galaxy mass that exceeds the typical value known in the nearby universe and aligns with that for JWST-detected unobscured AGNs. Consequently, we propose a hypothesis that the dust-rich environments in LRDs promote the emergence of rapidly spinning and overmassive BH populations.

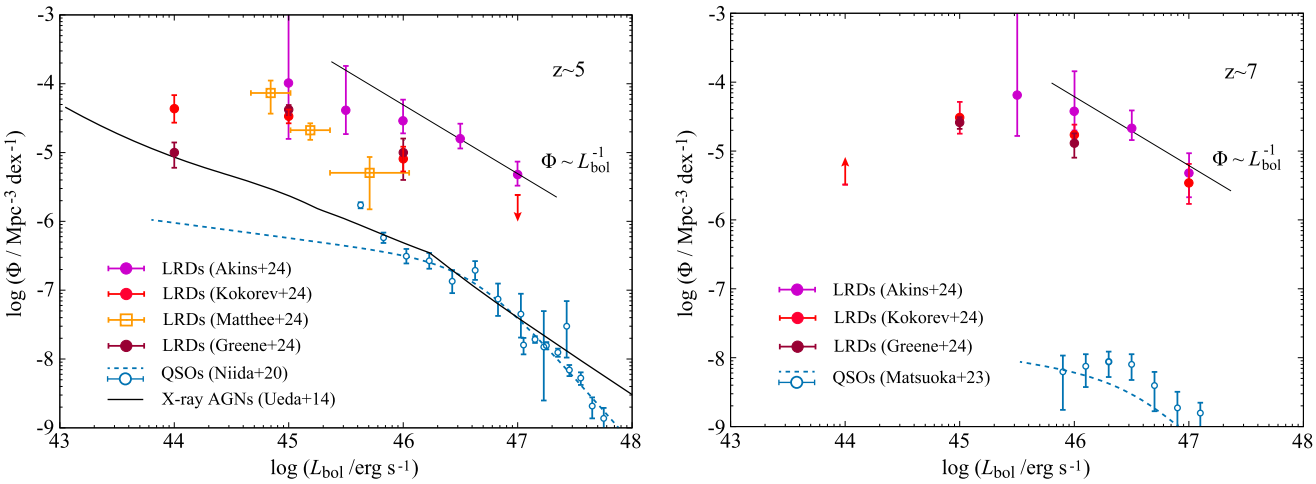

Figure 1. Bolometric AGN luminosity functions at $4.5 < z < 6$ (left) and $6.5 < z < 8.5$ (right). The luminosity function data obtained from different surveys are shown: the rest-UV-selected quasars (M. Niida et al. 2020; Y. Matsuoka et al. 2023), the X-ray-selected AGNs (Y. Ueda et al. 2014), and dust-reddened AGNs reported as "LRDs" identified with JWST photometry and slitless spectroscopy (H. B. Akins et al. 2024; J. E. Greene et al. 2024; J. Matthee et al. 2024; V. Kokorev et al. 2024). The bright-end slope of the LRD luminosity function is consistent with $\Phi \propto L_{\rm bol}^{-1}$ at both redshifts.

Throughout this Letter, we assume a flat Λ cold dark matter (CDM) cosmology consistent with the constraints from Planck (Planck Collaboration et al. 2020): $h = 0.6732$, $\Omega_{\rm m} = 0.3158$, $\Omega_\Lambda = 1 - \Omega_{\rm m}$, $\Omega_{\rm b} = 0.04938$, and $\sigma_8 = 0.8102$. It is important to note that observational studies referenced in our work have adopted a different set of cosmological parameters, $h = 0.7$ and $\Omega_{\rm m} = 0.3$. However, the differences in parameter choice have a negligible impact on the results.

2. Soltan Argument at $z \geqslant 5$

Early studies of LRDs have indicated that the observed values of $M_{\rm UV}$ are much fainter than the intrinsic UV magnitudes due to dust extinction (e.g., D. D. Kocevski et al. 2023; J. E. Greene et al. 2024; J. Matthee et al. 2024; V. Kokorev et al. 2024). To address the underlying AGN activity, these studies estimated bolometric AGN luminosity from rest-optical emissions. J. Matthee et al. (2024) and J. E. Greene et al. (2024) conducted JWST/NIRSpec observations on LRDs and converted the measured Hα luminosity to bolometric luminosity, while V. Kokorev et al. (2024) and H. B. Akins et al. (2024) relied on continuum luminosity L_{5100} and L_{3000} for a bolometric luminosity estimator, respectively, by assuming that all the continuum flux originates from the AGN. The AGN bolometric luminosity derived from the Hα luminosity, particularly its broad-line component emitted from fast-moving clouds near the AGN, is more accurate than using dust-dereddened continuum (see Section 4.3).

Figure 1 presents the bolometric luminosity functions at $z \simeq 5$ (left) and $z \sim 7$ (right), i.e., the number density per unit comoving volume per $\log L_{\rm bol}$ in units of $\mathrm{cMpc^{-3}\,dex^{-1}}$, combining data from various sources: rest-UV-selected unobscured quasars (M. Niida et al. 2020; Y. Matsuoka et al. 2023), X-ray-selected AGNs (Y. Ueda et al. 2014), and LRDs identified through JWST photometry and spectroscopy (H. B. Akins et al. 2024; J. E. Greene et al. 2024; J. Matthee et al. 2024; V. Kokorev et al. 2024).[4] For UV- and X-ray-selected AGNs, we adopt the bolometric correction factors calibrated by F. Duras et al. (2020). The abundance of unobscured quasars at $z \sim 5$ aligns closely with that of X-ray-detected AGNs for $L_{\rm bol} \gtrsim 4 \times 10^{45}\,\mathrm{erg\,s^{-1}}$, while the X-ray AGN abundance further increases at lower luminosity regimes.[5] This suggests that the obscured AGN fraction increases toward the fainter end (F. Vito et al. 2018). In contrast, LRDs exhibit a substantially greater abundance at $L_{\rm bol} \lesssim 10^{46}\,\mathrm{erg\,s^{-1}}$, nearly 1 order of magnitude above that of X-ray AGNs. While the LRD abundance data show some variations owing to differences in sample size and methods for estimating bolometric luminosity across the referred studies, the trend of overabundance relative to the other AGN populations is consistently observed. The bright-end slope of the LRD luminosity function is consistent with $\Phi \propto L_{\rm bol}^{-1}$ (H. B. Akins et al. 2024; V. Kokorev et al. 2024). Therefore, it is ensured that a large fraction of the production of radiation (i.e., the amount of material accreted to BHs) is dominated by these bright populations. The overabundance of LRDs and the bright-end slope of $\Phi \propto L_{\rm bol}^{-1}$ hold even at $z \gtrsim 7$.

In our analysis below, we consider abundance data from luminosity bins where the sample size is $N \geqslant 2$ but exclude bins with a sample size of $N = 1$. This approach aligns with Poisson statistical error estimates, where a single occurrence ($N = 1$) is statistically indistinguishable from zero. Additionally, for the COSMOS-Web luminosity function data, we exclude the data at the faint end of $L_{\rm bol} < 10^{46}\,\mathrm{erg\,s^{-1}}$ from H. B. Akins et al. (2024) since the COSMOS-Web survey is not deep enough to accurately measure the abundance of these faint populations and thus completeness correction matters.

Figure 2 illustrates the BH accretion rate density (BHAD) across various redshifts, with each data point and curve representing BHADs estimated under the assumption of a 10% radiative efficiency ($\epsilon_{\rm rad} = 0.1$). These include LRDs (H. B. Akins et al. 2024; J. E. Greene et al. 2024; J. Matthee et al. 2024; V. Kokorev et al. 2024) as well as X-ray-selected AGNs (J. Aird et al. 2015; T. T. Ananna et al. 2019;

[4] H. B. Akins et al. (2024) reported new LRD samples identified through the COSMOS-Web survey during the revision of our manuscript. The wide survey areas allow the detection of rarer and brighter LRD populations at $5 < z < 9$ and thus better constrain the abundance at the bright end.

[5] M. Niida et al. (2020) excluded the data at $M_{\rm UV} > -23.32$ mag, corresponding to the two faintest data points in the left panel of Figure 1, from their fitting because the contamination rate of point-like compact galaxies increases significantly toward the fainter regime.

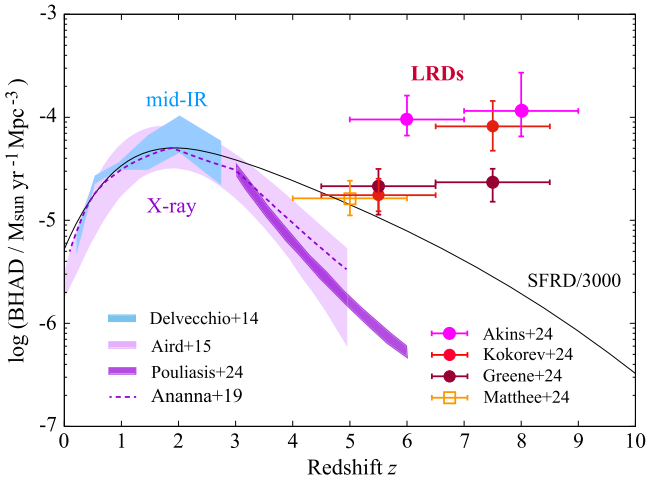

Figure 2. The cosmic BHAD as a function of redshift. Each data point and curve represents BHADs estimated under the assumption of a 10% radiative efficiency ($\epsilon_{\rm rad}=0.1$) for the three different populations, including LRDs (H. B. Akins et al. 2024; J. E. Greene et al. 2024; J. Matthee et al. 2024; V. Kokorev et al. 2024), X-ray-selected AGNs including Compton-thick populations (J. Aird et al. 2015; T. T. Ananna et al. 2019; E. Pouliasis et al. 2024), and mid-infrared-selected AGNs (I. Delvecchio et al. 2014). For comparison, the cosmic SFRD scaled by a factor of 3000 is overlaid (Y. Harikane et al. 2022). The BHAD attributed to LRDs remains significantly dominant at $z>6$.

E. Pouliasis et al. 2024) and mid-infrared-selected AGNs (I. Delvecchio et al. 2014). The BHAD estimated from X-ray sources including Compton-thick AGN contributions agrees well to that of mid-infrared AGNs at $z\sim3$. With the same value of $\epsilon_{\rm rad}=0.1$, the BHAD inferred from the bolometric luminosity function of LRDs indicates a persistent or even increasing trend toward higher redshifts ($4<z<8.5$), opposite to the declining trend of X-ray-selected AGNs. Note that completeness corrections for some LRD samples we adopt (e.g., J. Matthee et al. 2024; V. Kokorev et al. 2024) have not been fully implemented in estimating the abundance of faint sources, thereby potentially leading to an increased abundance at the faint sources. Nevertheless, our finding is unlikely to alter because the brighter LRD populations dominantly contribute to the BHAD (i.e., $d\log\Phi/d\log L_{\rm bol}\simeq-1$). Note that the BHAD estimated from the COSMOS-Web result increases by <20% when faint AGNs with $L_{\rm bol}<10^{46}\,{\rm erg\,s^{-1}}$ are included in our analysis.

For comparison, we overlay the cosmic star formation rate density (SFRD) scaled by a factor of 3000 (Y. Harikane et al. 2022). The scaled SFRD matches well with the BHAD based on the mid-infrared-selected AGNs at $z\lesssim3$ and appears to be consistent with the BHAD of LRDs at $z\simeq5$–6. On the other hand, the BHAD attributed to LRDs remains significantly dominant at $z>6$. This finding, based on the assumption of $\epsilon_{\rm rad}=0.1$, indicates that rapid growth of BHs at these earlier epochs established a trend of overmassive BH in terms of the $M_\bullet/M_\star$ ratio, as observed in recent JWST AGN studies at $z>6$ (e.g., F. Pacucci et al. 2023; R. Maiolino et al. 2023; Y. Harikane et al. 2023).

In the left panel of Figure 3, we show the evolution of the BH mass density within a comoving volume throughout cosmic time. The solid curve represents the cumulative BH mass density deduced from the AGN bolometric luminosity functions (primarily X-ray-selected populations) at $0<z<5$, under an assumed 10% radiative efficiency (Y. Ueda et al. 2014). This projection agrees closely with the observed BH mass density at $z\simeq0$ (F. Shankar et al. 2009), concluding the plausibility of the preassumed radiative efficiency ($\epsilon_{\rm rad}=0.1$; A. Sotan 1982; Q. Yu & S. Tremaine 2002). Additionally, we present the BH mass density directly derived from the integration of the BHMF for LRDs at $z\simeq5$, estimated to be $\rho_\bullet\simeq2.8^{+2.2}_{-1.2}\times10^3\,M_\odot\,{\rm cMpc^{-3}}$ (red symbols; J. E. Greene et al. 2024; J. Matthee et al. 2024; V. Kokorev et al. 2024).[6] This estimate remarkably aligns with expectations based on the Soltan argument assuming the conventional radiative efficiency of 10% at $0<z<5$, further reinforcing the consistency across the three distinct physical measures.

Next, we extend our analysis to the universe at $z>5$, focusing on the cumulative mass of BHs accreted during the LRD phase, $\Delta\rho_\bullet\equiv{\rm BHAD}\times\Delta t$, calculated from their bolometric luminosity function over a redshift interval. We categorize the LRD samples into two groups: those identified through the COSMOS-Web survey (magenta; H. B. Akins et al. 2024) and LRDs from other observational programs (blue; J. E. Greene et al. 2024; J. Matthee et al. 2024; V. Kokorev et al. 2024). This classification is based on two considerations: (1) the redshift intervals different among the samples in the literature, requiring a uniform redshift bin size for comparative analysis; (2) the need to evaluate the impact of wide-area surveys such as COSMOS-Web on the LRD Soltan argument. As seen in the left panel of Figure 3, one can find the cumulative mass of BHs at $z>5$ substantially exceeds the observed mass density at $z\simeq5$ as well as the predictions from a BH growth model calibrated with UV- and X-ray-selected AGN luminosity functions (dotted curve; W. Li et al. 2024a). This discrepancy raises concerns about a potential violation of the BH mass conservation law; namely, $\rho_\bullet(z\simeq5)\gtrsim\Delta\rho_\bullet(z>5)$ needs to be held. Thus, the possible inapplicability of $\epsilon_{\rm rad}=0.1$ is suggested for the early universe beyond $z>5$. Adjusting the radiative efficiency upward impacts the inferred BHAD, which follows $\propto(1-\epsilon_{\rm rad})/\epsilon_{\rm rad}$. For instance, adopting the theoretical upper limit of $\epsilon_{\rm rad}=0.42$ for an extreme Kerr BH with a spin parameter $a_\bullet=1$ (e.g., R. P. Kerr 1963; I. D. Novikov & K. S. Thorne 1973) resolves the discrepancy between the integrated BHMF values and the cumulative mass derived from the BHAD. The relationship between the radiative efficiency and BH spin is well understood for geometrically thin accretion disks, where a thermal equilibrium is maintained through efficient radiative cooling that balances with viscous heating (N. I. Shakura & R. A. Sunyaev 1973). However, this scenario changes in low-accretion-rate states, where the disk becomes geometrically thick due to *inefficient* cooling (e.g., F. Yuan & R. Narayan 2014). In such cases, the radiative efficiency substantially decreases from the values in the thin-disk approximation (K. Inayoshi et al. 2019). This reduction in $\epsilon_{\rm rad}$ enlarges the discrepancy between $\rho_\bullet(z\simeq5)$ and $\Delta\rho_\bullet(z>5)$ rather than mitigating it.

The right panel of Figure 3 provides a detailed quantitative comparison of BH mass density values from several studies, using the least-squares method for fitting $\rho_\bullet$ and $\Delta\rho_\bullet$ at each redshift interval. The cumulative values of $\Delta\rho_\bullet$ across the entire redshift range are denoted by star symbols for each LRD sample (see also Table 1). For the case without the COSMOS-

[6] We note that the BHMF from the LRD samples in V. Kokorev et al. (2024) is derived from their AGN bolometric luminosity function, assuming an average Eddington ratio value $\langle\lambda_{\rm Edd}\rangle\simeq0.3$, which is motivated by the samples of broad-line LRDs compiled by J. E. Greene et al. (2024).

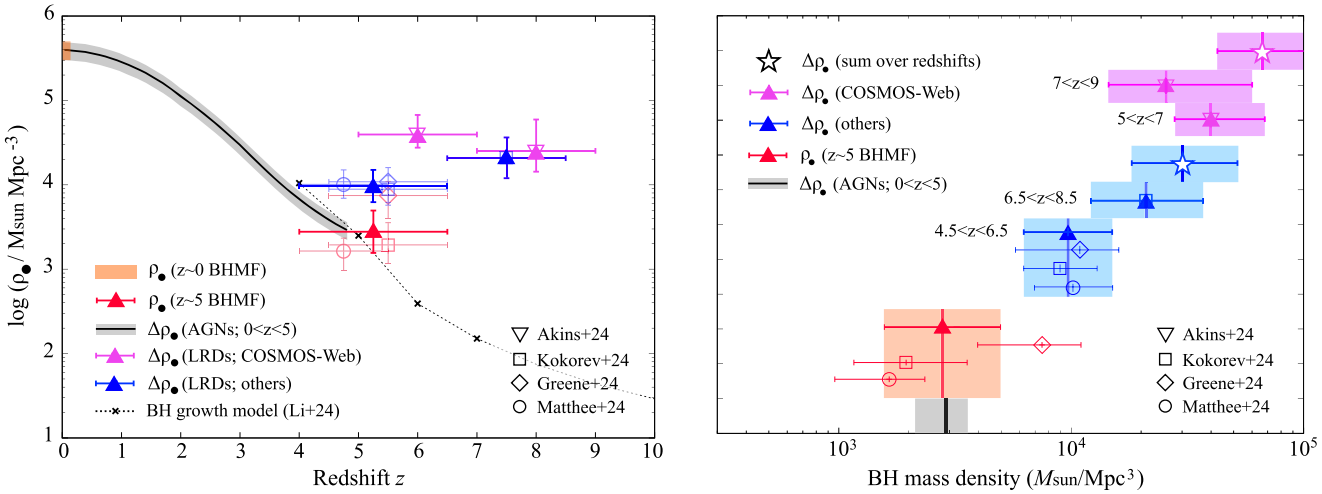

Figure 3. Left: Cosmic evolution of the BH mass density in a comoving volume. At $z \sim 5$, the BH mass density is derived from the integration of the BHMF for LRDs (red symbols). From this point, the mass density grows toward lower redshifts following the BHAD deduced from known AGN populations with a 10% radiative efficiency (solid curve; Y. Ueda et al. 2014) and reaches the density of relic BHs in the nearby universe (F. Shankar et al. 2009). At $z > 5$, the cumulative mass accreted to BHs during the LRD phase, $\Delta\rho_\bullet \equiv \mathrm{BHAD} \times \Delta t$ inferred from their bolometric luminosity function over a time span Δt for given redshift range based on the COSMOS-Web (magenta) and the other surveys (blue), assuming a 10% radiative efficiency, substantially exceed the observed mass density at $z \simeq 5$ as well as the predictions from a BH growth model calibrated with UV and X-ray selected AGN luminosity function (dotted curve; W. Li et al. 2024a). Data for LRDs are derived from luminosity functions and BH mass estimates provided in the literature (open symbols, H. B. Akins et al. 2024; J. E. Greene et al. 2024; J. Matthee et al. 2024; V. Kokorev et al. 2024) and the mean values for each group (filled symbols). Right: Summary of the BH mass density and the cumulative mass density during the LRD phase assuming a 10% radiative efficiency. Shaded areas indicate the BH mass density $\rho_\bullet$ at $z \simeq 5$ (red) and the cumulative mass density accrued during the LRD stage calculated from the COSMOS-Web (magenta) and the other surveys (blue). The total sum of $\Delta\rho_\bullet$ over the entire redshift range in each data group is shown with a star symbol.

Table 1
Significance of the Difference between $\rho_\bullet(z \simeq 5)$ and $\Delta\rho_\bullet(z \gtrsim 5)$ for Different Radiative Efficiencies

Survey	Redshift	$\log_{10}\Delta\rho_\bullet$	*p*-value			
...	...	$\epsilon_{\rm rad} = 0.1$	$\epsilon_{\rm rad} = 0.1$	$\epsilon_{\rm rad} = 0.2$	$\epsilon_{\rm rad} = 0.3$	$\epsilon_{\rm rad} = 0.42$
...	...	$a_\bullet \simeq 0.674$	$a_\bullet \simeq 0.674$	$a_\bullet \simeq 0.960$	$a_\bullet \simeq 0.996$	$a_\bullet \simeq 1.00$
COSMOS-Web	$5 < z < 9$	$4.82^{+0.29}_{-0.19}$	0.00204	0.00569	0.0132	0.0350
Other surveys	$4.5 < z < 8.5$	$4.48^{+0.24}_{-0.22}$	0.00291	0.0115	0.0378	0.151

Note. Column (1): survey. Column (2): redshift ranges. Column (3): cumulative mass density of BHs accreted during the LRD phase (in units of $M_\odot$ cMpc^{-3}) with a 10% radiative efficiency. Column (4)–(7): the *p*-value evaluated in the *t*-test for the null hypothesis between $\rho_\bullet(z = 5)$ and $\Delta\rho_\bullet$ at $z > 5$ for different values of the radiative efficiency (and the corresponding BH spin parameters). Here, we consider two cases with LRD data based on the COSMOS-Web survey (H. B. Akins et al. 2024) and other LRD surveys (J. E. Greene et al. 2024; J. Matthee et al. 2024; V. Kokorev et al. 2024) for calculating the total cumulative mass. The COSMOS-Web result requires $\epsilon_{\rm rad} \geqslant 0.2$ beyond the $>3\sigma$ confidence level, while the confidence level is $\gtrsim 2\sigma$ with LRD samples from other surveys.

Web survey (blue symbols), the accreted mass density at $z \sim 5$ is found to be lower than that at $z \sim 7$. This difference is primarily due to the finding of V. Kokorev et al. (2024), where $N = 9$ luminous LRDs with $L_{\rm bol} \simeq 10^{47}$ erg s^{-1} were identified at $6.5 < z < 8.5$, but only one was reported at $4.5 < z < 6.5$ within a large sample set of LRDs from multiple survey fields. We note that luminosity function bins with a sample size of $N = 1$ are excluded in our analysis as a single occurrence is statistically indistinguishable from zero. Therefore, the inclusion of these luminous populations substantially influences the BHAD estimate. Using only the COSMOS-Web result (magenta symbols), we consistently observe higher values of $\Delta\rho_\bullet$ at the two redshift ranges, owing to the wide-area survey designed to identify more luminous and rarer populations. As a result, the total sum in each case reaches as high as $\Delta\rho_\bullet \simeq 3.0^{+2.2}_{-1.2} \times 10^4$ and $6.6^{+6.3}_{-2.3} \times 10^4\, M_\odot$ cMpc^{-3}, respectively (star symbol). With the mean values, the cumulative mass densities during the LRD phases over $5 < z < 9$ appear to be $\gtrsim 10$ times higher than the BH mass density at $z \simeq 5$. However, there is a concern regarding the classification of both the LRD samples of V. Kokorev et al. (2024) and H. B. Akins et al. (2024), where all photometrically selected LRDs are considered as AGNs due to the lack of spectroscopic observations (see also Section 4.3). Due to these concerns, the cumulative mass density of BHs and their difference from the BH mass density are considered to be upper bounds.

To understand the influence of each contribution of $\Delta\rho_\bullet$ on this analysis and the need for a radiative efficiency beyond the standard 10% value, we explore two scenarios: one considering the contribution from the COSMOS-Web survey (magenta) and another one compiling LRD samples from other observational programs (blue). In this work, to assess the statistical difference between $\rho_\bullet(z \simeq 5)$ and $\Delta\rho_\bullet$ for each of the two cases, we employ the *t*-test, which serves as an appropriate statistical method to determine whether there is a statistically significant difference in the mean values between two groups with unequal sample variances. The *p*-values, as summarized in Table 1, indicate that the hypothesis of agreement between the two quantities at $\epsilon_{\rm rad} = 0.1$ is statistically rejected in the two cases with a confidence level of $>99.7\%$ ($p < 0.003$). For the

analysis with the COSMOS-Web survey result, a radiative efficiency greater than $\epsilon_{\rm rad} \geqslant 0.3$ is concluded with a confidence level of >98%, while the case with other LRD survey data suggests $\epsilon_{\rm rad} \geqslant 0.2$ with a similar confidence level. This finding suggests that the majority of BHs within LRDs or similarly gas-/dust-rich environments are likely to process rapid spins with an average $\epsilon_{\rm rad} \geqslant 0.2$–0.3 (the corresponding BH spin is $a_\bullet \simeq 0.96$–0.996), indicating a prevalent condition of rapid angular momentum in BH growing environments in the early universe.

This result suggests that BH growth at these high redshifts, especially in LRDs, is likely dominated by prolonged accretion episodes with coherent angular momentum directions or a modest degree of anisotropy (e.g., M. Volonteri et al. 2005; M. Dotti et al. 2013), unlike short-lived chaotic accretion with randomly oriented inflows that tend to spin BHs down (e.g., A. R. King et al. 2008). Our conclusion on rapid spins of the early BH population will be directly testable through future gravitational-wave observations with space-based detectors such as LISA, TianQin, and Taiji (e.g., P. Amaro-Seoane et al. 2023; A. Torres-Orjuela et al. 2024).

Intriguingly, clustering analyses of quasars and galaxies at $z \gtrsim 6$ suggest that the duty cycle of UV-bright quasars is as low as $\lesssim$1% (A. -C. Eilers et al. 2024; E. Pizzati et al. 2024), corresponding to a quasar lifetime of 1–10 Myr, which is significantly shorter than the e-folding time assuming the Eddington accretion rate. This finding implies that most of the BH mass growth would have occurred in highly (UV-) obscured environments and/or through episodic super-Eddington phases with a lower radiative efficiency (F. B. Davies et al. 2019; see also K. Inayoshi et al. 2016, 2022b). The first implication is consistent with the hypothesis that LRDs are moderately obscured AGNs (e.g., Z. Li et al. 2024b). The second implication, concerning the potential mass contribution from radiatively inefficient super-Eddington growth, would be constrained by our findings in this work and is left for future investigations.

3. Potential Overmassive BH Trends in LRDs

In this section, we explore the possibility that BHs within LRDs are overmassive relative to the mass correlation with their host mass, as implied from the BHAD-to-SFRD ratio shown in Figure 2. In general, estimating the stellar mass of dust-obscured sources poses a significant challenge in the absence of rest-frame near-infrared data provided by JWST MIRI (e.g., C. C. Williams et al. 2024; P. G. Pérez-González et al. 2024). Instead of examining the detailed spectral energy distribution fitting analysis, we focus on putting an upper bound for the stellar mass. This approach ensures that the observed abundance of LRDs does not exceed the theoretical upper bound in the standard ΛCDM model with a 100% conversion efficiency from gas to stars (e.g., M. Boylan-Kolchin 2023).

The stellar continuum for LRDs can be constrained by the dust-corrected continuum flux at 5100 Å. Given that broad Hα emission indicates AGN dominance in the continuum (see Section 4.3), we adjust $L_{\star,5100} = f_L L_{5100}$, where f_L is significantly less than unity. To estimate an upper bound of stellar mass, we employ the STARBURST99 population synthesis code (version 7.0.1; C. Leitherer et al. 1999), adopting a Kroupa initial mass function (IMF; P. Kroupa 2001; 0.1–100 $M_\odot$), Padova isochrone models, constant star formation, and solar metallicity. This approach yields a galaxy mass−luminosity relation of

$$\frac{M_\star}{10^9\,M_\odot} \simeq 1.3\,f_{\rm IMF}\left(\frac{L_{\star,5100}}{10^{43}\ {\rm erg\ s^{-1}}}\right)\left(\frac{t_{\rm age}}{1\ {\rm Gyr}}\right), \quad (1)$$

which is applicable for stellar ages of $t_{\rm age} \sim 0.3$–3 Gyr. This estimate is sensitive to the low-mass end of the stellar IMF ($f_{\rm IMF} = 1$ for $m_{\star,\rm min} = 0.1\,M_\odot$); for instance, setting the minimum mass up to $m_{\star,\rm min} = 1.0\,M_\odot$ decreases the factor to $f_{\rm IMF} \sim 0.3$.

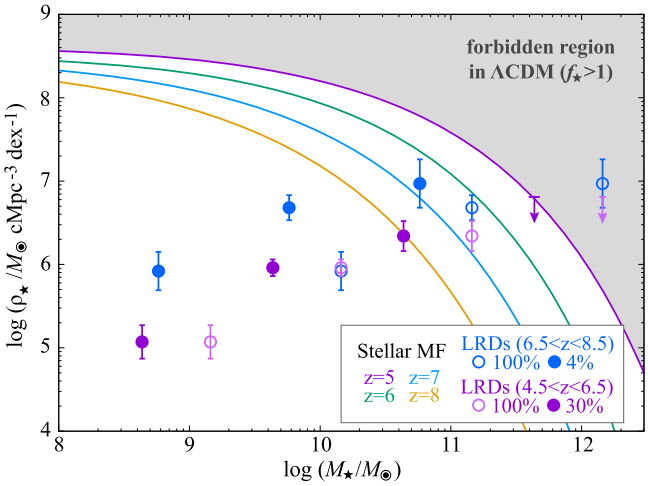

Figure 4. Stellar mass density in galaxies hosting LRDs at various redshifts, calculated using Equation (1) and assuming $\mathscr{F}(\equiv f_{\rm IMF}\,f_L) = 1.0$ (open symbols) at two redshift ranges of $4.5 < z < 6.5$ and $6.5 < z < 8.5$. For comparison, the stellar mass function derived from the DM halo mass function at $5 \leqslant z \leqslant 8$ is shown with a 100% star formation efficiency. An upper bound of the stellar mass constrains $\mathscr{F} < 0.3 f_\star$ for $4.5 < z < 6.5$ and $\mathscr{F} < 0.04 f_\star$ for $6.5 < z < 8.5$ (filled symbols).

Figure 4 presents the stellar mass function (in units of $M_\odot\,{\rm cMpc}^{-3}$) in galaxies hosting LRDs at various redshifts, calculated by using Equation (1) and assuming $\mathscr{F}(\equiv f_{\rm IMF}\,f_L) = 1.0$ at two redshift ranges of $4.5 < z < 6.5$ and $6.5 < z < 8.5$ (open circles), based on the LRD luminosity function obtained by V. Kokorev et al. (2024). Since the luminosity function of LRDs follows $\Phi \propto L_{\rm bol}^{-1}$, the stellar mass density becomes flatter at the high-mass end when the stellar mass is translated from the luminosity with Equation (1). We compare the results to the stellar mass function derived from the halo mass function at $5 \leqslant z \leqslant 8$, assuming $M_\star = f_\star f_{\rm b} M_{\rm h}$, where $f_{\rm b} = 0.16$ is the cosmic baryon fraction and $f_\star$ is the star formation efficiency (see more details in K. Inayoshi et al. 2022a). Setting $f_\star = 1.0$ offers a theoretical upper limit on stellar mass in galaxies ($f_\star > 1$; the forbidden region), highlighting a mismatch between the stellar mass density contained in LRDs with $\mathscr{F} = 1.0$ and the ΛCDM upper limit. As a result, we deduce a stringent constraint denoted with filled circles:

$$\mathscr{F} < 0.3\,f_\star \ \ {\rm at}\ \ 4.5 < z < 6.5,$$
$$\mathscr{F} < 0.04\,f_\star \ \ {\rm at}\ \ 6.5 < z < 8.5. \quad (2)$$

Figure 5 shows the $M_\bullet - M_\star$ distribution for high-redshift AGNs, including LRDs (square), JWST-detected unobscured AGNs (cross), and quasars identified in ground-based surveys (circle). For the LRDs at $4.5 < z < 6.5$ (red) and $6.5 < z < 8.5$ (orange), we derive the stellar mass of those with broad Hα emission from J. E. Greene et al. (2024) using Equation (1). This calculation incorporates the upper limit for the stellar continuum ratio $\mathscr{F}$ to the observed continuum (see

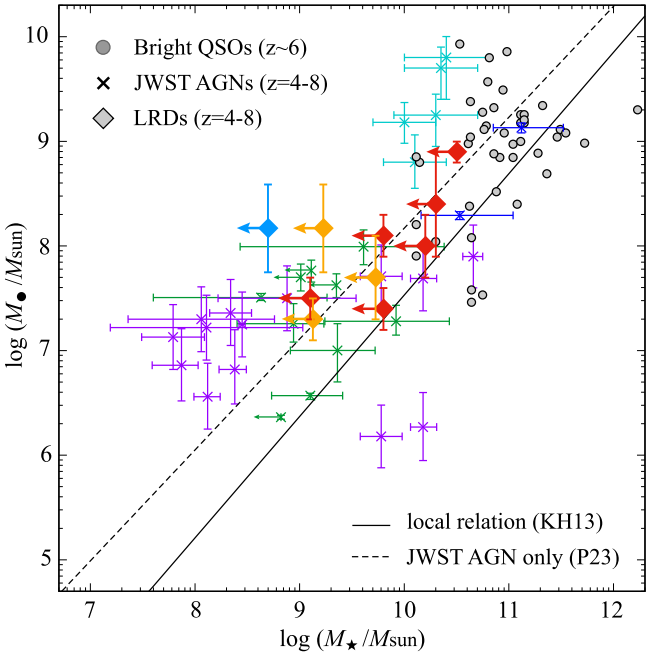

Figure 5. $M_\bullet - M_\star$ distribution for high-redshift AGNs, including LRDs, JWST-detected unobscured ANGs at $z = 4$–8 (purple, R. Maiolino et al. 2023; green, Y. Harikane et al. 2023; cyan, M. A. Stone et al. 2024; and blue, X. Ding et al. 2023), and quasars identified in ground-based surveys (T. Izumi et al. 2021). For the LRDs at $4.5 < z < 6.5$ (red) and $6.5 < z < 8.5$ (orange), we derive the upper bound of the stellar mass based on the dust-corrected continuum flux measured by J. E. Greene et al. (2024) using Equations (1) and (2). Additionally, a $z = 8.5$ LRD with broad Hβ emission, for which the stellar mass is constrained by ALMA nondetections, is overlaid (blue; V. Kokorev et al. 2023). Two different mass correlations are overlaid: the local relationship (solid; J. Kormendy & L. C. Ho 2013) and the JWST-detected AGNs (dashed; F. Pacucci et al. 2023).

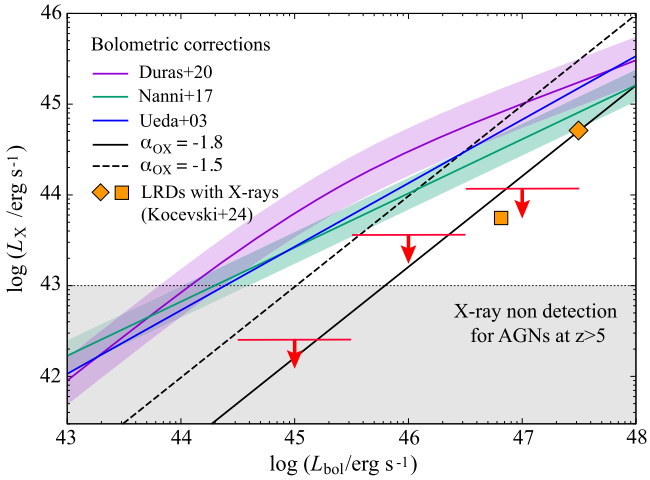

Figure 6. The critical X-ray luminosities for LRDs at $z \sim 5$, determined by the requirement for LRDs not to be classified as X-ray AGNs nor contributing to the abundance of X-ray AGNs (red horizontal lines with arrows). For comparison, several models for bolometric correction to X-rays are shown (Y. Ueda et al. 2003; R. Nanni et al. 2017; F. Duras et al. 2020), as well as the cases with constant optical-to-X-ray spectral indices of $\alpha_{OX} = -1.5$ (dashed) and -1.8 (solid). The $L_{bol} - L_X$ values of the two LRDs detected in X-rays are shown with orange symbols; JADES 21925 (square) and PRIMER-COS 3982 (diamond; D. D. Kocevski et al. 2024). The shaded area denotes X-ray luminosities below the detection threshold of current Chandra observations for JWST fields.

Equation (2) and Figure 4), ensuring consistency with the theoretical upper bound of stellar mass density in the ΛCDM universe. The $M_\bullet - M_\star$ values for LRDs tend to be overmassive compared to the local relationship (solid line; J. Kormendy & L. C. Ho 2013), and they align well with other AGNs detected by JWST and follow the mass correlation inferred from JWST AGN data, excluding quasars from ground-based surveys (dashed line; F. Pacucci et al. 2023). Moreover, their distribution is consistent with the locus of a JWST/NIRSpec-confirmed $z = 8.5$ LRD that exhibits broad Hβ emission, for which an upper limit on the stellar mass has been constrained by nondetection in Atacama Large Millimeter/submillimeter Array (ALMA) observations (blue; V. Kokorev et al. 2023).

The mass ratios for these LRDs are also consistent with the BHAD/SFRD values at $z > 6$ shown in Figure 2. This suggests a model in which transient rapid growth phases during the LRD stages elevate these BHs into an overmassive state. This hypothesis is supported both theoretically (e.g., K. Inayoshi et al. 2022b; H. Hu et al. 2022) and observationally (S. Fujimoto et al. 2022), providing a comprehensive insight into the BH growth dynamics in the early universe.

4. Discussion

4.1. Missing X-Ray Radiation from LRDs

X-ray AGN surveys are generally effective in identifying obscured AGNs. However, in the case of LRDs observed with JWST, no X-ray counterparts have been reported in early studies (e.g., D. D. Kocevski et al. 2023; L. J. Furtak et al. 2023; J. Matthee et al. 2024). X-ray weakness has been consistently observed in LRDs, as demonstrated by stacking analyses (M. Yue et al. 2024), and this phenomenon extends beyond LRDs to a more general category of unobscured broad-line AGNs (R. Maiolino et al. 2024). Further emphasizing the rarity of X-ray emissions, D. D. Kocevski et al. (2024) have identified only two X-ray-detected LRDs at $z = 3.1$ and 4.66 among 341 examined objects, resulting in a detection fraction of less than 0.6 %. The optical continuum extinction measurements suggest a gas column density of $N_H \sim 3.3 \times 10^{22} (A_V/3.0) \mathrm{cm}^{-2}$ (R. Maiolino et al. 2001), indicating that the column density outside the broad-line region is too low to obscure X-rays. The column density estimate is broadly consistent with those measured from the X-ray spectral analysis for the two X-ray-detected LRDs, $N_H \sim (5-20) \times 10^{22} \mathrm{cm}^{-2}$ (D. D. Kocevski et al. 2024).

Considering the absence of X-ray counterparts for LRDs, we explore the possibility that their X-ray emission is intrinsically weak, as compared to typical X-ray selected AGNs. Figure 6 presents the critical X-ray luminosity for each bolometric luminosity, so that $\Phi_X(L_{X,crit}) \geqslant \Phi_{LRD}(L_{bol})$, where we adopt the X-ray AGN luminosity function Φ_X from Y. Ueda et al. (2014) and the LRD bolometric luminosity function Φ_{LRD} from V. Kokorev et al. (2024). This condition requires that LRDs must have a bolometric correction factor to X-rays that prevents them from being classified as X-ray AGNs and contributing to their abundance (red horizontal lines with arrows). The critical X-ray luminosity is limited below those derived from comparison between the X-ray- and optical-based AGN luminosity functions at lower redshifts of $z \lesssim 2$ (Y. Ueda et al. 2003).

To quantify this intrinsic X-ray faintness in LRDs, we utilize the optical-to-X-ray spectral index, defined as $\alpha_{OX} = \log(L_{\nu,2keV}/L_{\nu,2500})/\log(\nu_{2keV}/\nu_{2500})$, where $L_{\nu,2keV}$ and $L_{\nu,2500}$ are the extinction-corrected luminosity density at

2 keV and 2500 Å, respectively. Our findings support a constant value of $\alpha_{\rm OX}$ lower than -1.8 rather than the luminosity-dependent $\alpha_{\rm OX}$ values observed in unobscured quasars across $0 \lesssim z \lesssim 6$ (e.g., A. T. Steffen et al. 2006; F. Duras et al. 2020). The upper bound of $\alpha_{\rm OX} \simeq -1.8$ is seen in the most luminous quasar populations with $L_{\rm bol} \gtrsim 10^{47}\,{\rm erg\,s^{-1}}$ (R. Nanni et al. 2017), which does not apply to most LRDs studied in this Letter.

The extensive LRD samples by V. Kokorev et al. (2024), consisting of 260 dust-reddened AGN candidates, are compiled from deep JWST/NIRCam fields totaling ∼340 arcmin^2. This includes observations from the CEERS field, which spans ∼51.9 arcmin^2 and falls within the coverage area of the Chandra AEGIS-XD survey coverage (K. Nandra et al. 2015). The survey detection limit reaches $1.5 \times 10^{-16}\,{\rm erg\,s^{-2}\,cm^{-1}}$ at 0.5–10 keV, which corresponds to $L_{\rm X} \simeq 1.1 \times 10^{43}\,{\rm erg\,s^{-1}}$ at the rest frame of 2–10 keV for $z \sim 5$–7 sources assuming a photon index of $\Gamma = -1.7$ and a Compton-thin limit ($N_{\rm H} < 10^{24}\,{\rm cm^{-2}}$). Given the average surface density of these LRDs (≃0.77 arcmin^{-2}), ∼40 LRDs in the CEERS field show no X-ray detection above this threshold. This suggests that nondetection of X-rays among LRDs can be explained by the intrinsic faintness of X-rays, as shown in Figure 6. Nevertheless, the most luminous LRDs with $L_{\rm bol} \gtrsim 10^{47}\,{\rm erg\,s^{-1}}$ might still be observed in X-rays unless classified as Compton-thick AGNs. Additionally, we note that the two LRDs detected in X-rays with a modest hydrogen column density of $N_{\rm H} \sim 10^{23}\,{\rm cm^{-2}}$ show obscuration-corrected X-ray luminosities of $L_{\rm X} \simeq 5.4 \times 10^{43}\,{\rm erg\,s^{-1}}$ (for JADES 21925 at $z_{\rm photo} = 3.1$) $L_{\rm X} \simeq 5.0 \times 10^{44}\,{\rm erg\,s^{-1}}$ (for PRIMER-COS 3982 at $z_{\rm spec} = 4.66$), respectively (D. D. Kocevski et al. 2024). The bolometric luminosities calculated from the rest-optical fluxes are $L_{\rm bol} \simeq 6.5 \times 10^{46}\,{\rm erg\,s^{-1}}$ and $3.1 \times 10^{47}\,{\rm erg\,s^{-1}}$ after dust attenuation correction. These findings also suggest a lower value of $\alpha_{\rm OX} \simeq -1.8$, as shown in Figure 6 (orange symbols).

Alternatively, if the X-ray emission was not intrinsically faint (except the two X-ray detected LRDs), most of these LRDs would be embedded in Compton-thick gas with $N_{\rm H} \gg 10^{24}\,{\rm cm^{-2}}$, concealing the LRDs from deep X-ray observations. However, such high densities are not expected in the LRD rest-optical spectra, which show a modest extinction $A_{\rm V} \sim 3$ mag, equivalent to $N_{\rm H} \sim 3 \times 10^{22}\,{\rm cm^{-2}}$. This discrepancy is also consistent with the lack of expected absorption features in their NIRSpec rest-frame UV spectra of LRDs with broad-emission lines (e.g., J. E. Greene et al. 2024).

4.2. Dusty Young Starburst Galaxies Mimicking LRD-like AGNs?

The classification of LRDs as AGNs has relied on the detection of broad Hα emission. However, such high-velocity gas can also originate from stellar processes, such as stellar winds or supernova explosions. Wolf–Rayet (WR) galaxies, characterized by young and massive stellar populations, can exhibit broad Hα emission as well as other high-ionization lines (e.g., L. C. Ho et al. 1995; D. Schaerer et al. 1999). Therefore, to conclusively confirm the AGN nature of LRDs, it is essential to perform line diagnostics that extend beyond simply identifying broad Hα emission, e.g., detection of broad He II λ4686 emission, a signature frequently associated with WR galaxies (e.g., NGC 4214 discussed in W. L. W. Sargent & A. V. Filippenko 1991).

Spectroscopic observations provide valuable insights into the characteristics of emission lines in LRDs. Initial studies by D. D. Kocevski et al. (2023) and J. E. Greene et al. (2024) have found that the He II λ4686 line, commonly associated with WR stellar activity, is absent in these LRD sources. Additionally, the spectral signatures typically linked to WR stars have not been observed within the LRD samples. The lack of He II and other WR-indicative spectral lines suggests that the broad Hα emissions detected in LRDs are not of stellar origin (note that detection of He II λ4686 does not necessarily exclude the AGN possibility because the emission is also observed in AGNs). This finding supports the hypothesis that AGNs are responsible for these emissions. More detailed spectroscopic analyses of multiple emission lines would strengthen this conclusion (J. E. Greene et al. 2020; A. E. Reines 2022).

4.3. Bolometric Luminosity Estimates

Our study is motivated by intriguing discoveries on the high abundance of LRDs, but an important consideration about the AGN luminosity estimate needs to be noted. While the UV luminosity functions show similar shapes across different studies, significant variations in the bolometric luminosity function arise due to the different methods used for bolometric luminosity estimates (see Figure 1). Since the observed rest-frame UV flux is heavily attenuated, earlier studies have employed either the rest-frame continuum flux at 5100 Å(V. Kokorev et al. 2024) or the direct Hα emission luminosity, when available, as a proxy for the AGN bolometric luminosity (J. E. Greene et al. 2024; J. Matthee et al. 2024).

The approach that relies on continuum flux introduces uncertainties of determining the AGN contribution to the total flux, which might result in overestimated luminosity. Furthermore, the selection of LRDs based solely on photometric criteria might include non-AGN sources such as Galactic brown dwarfs (D. Langeroodi & J. Hjorth 2023), thereby possibly overestimating the AGN abundance. J. E. Greene et al. (2024) reported the identification success rate of AGNs among LRDs in the UNCOVER field to be approximately 60%. V. Kokorev et al. (2024) studied LRDs based on the photometric data from multiple JWST survey areas, using color selection conditions provided by J. E. Greene et al. (2024), which effectively remove contaminants of Galactic brown dwarfs. To date, other types of low-z interlopers, such as Balmer break galaxies, for LRDs have not been reported via spectroscopic studies.

In contrast, spectroscopic data, particularly with measurements of broad Hα emission, facilitate confirmation of the AGN presence and a more accurate determination of $L_{\rm bol}$. This method adopts an empirical relationship derived from local AGN observations (J. E. Greene & L. C. Ho 2005). For LRD sources with detected Hα emissions, the continuum fluxes at 5100 Å calculated through the two methods yield ratios of $L_{5100,{\rm H}\alpha}/L_{5100,{\rm c}} \simeq 1.2 \pm 0.2$ (J. E. Greene et al. 2024). This result supports the scenario that the continuum emission at 5100 Å is substantially AGN origin, not from the dust-reddened stellar continuum of the host galaxy (i.e., $f_L \ll 1$).

One limitation in the work by J. E. Greene et al. (2024) is the use of low-resolution PRISM spectra for analyzing Hα emissions, which complicates the decomposition of broad and narrow Hα emissions in some cases. To address this challenge, we can use an empirical relationship obtained through higher-resolution spectroscopic observations by

J. Matthee et al. (2024). This relationship examines the flux ratio between narrow and broad Hα emissions in LRDs; namely, the ratio $F_{\mathrm{H}\alpha,\mathrm{broad}}/F_{\mathrm{H}\alpha,\mathrm{tot}}$ exceeds 0.6 with a positive rest-frame optical spectral index, with the ratio approaching unity as the spectral index increases. Therefore, the potential systematic errors in estimating broad Hα line luminosity due to incomplete spectral line decomposition could be alleviated by employing this relationship.

Despite these complexities found in current analyses, the central conclusion of our discussion remains valid on a qualitative level. Nevertheless, the development of more quantitative arguments will benefit from further observational explorations that refine the understanding of the AGN characteristics of LRDs and provide a more precise estimate of their cosmic abundance (e.g., Z. Li et al. 2024b).

4.4. Multimessenger Counterparts

In this study, we propose a scenario where the dust-rich environments within LRDs lead to the emergence of rapidly spinning and overmassive BHs. The high spins of these BHs may yield a strong correlation between the presence of relativistic jets (e.g., R. D. Blandford & R. L. Znajek 1977), high-energy emissions and particles (e.g., L. Dai & K. Fang 2017; K. Murase et al. 2020), and transient bursts such as stellar tidal disruption events (e.g., K. Inayoshi et al. 2024), with early BHs being overmassive compared to the mass correlation observed in the nearby universe.

Multiwavelength surveys including radio, optical, and X-ray bands have reported that the radio powers (or radio loudness) of obscured AGNs initially identified by the Very Large Array/Faint Images of the Radio Sky at Twenty-Centimeters survey as bright radio sources tend to increase with redshifts at $0.5 < z < 3.5$, with jet powers exceeding $P_{\mathrm{jet}} \gtrsim 10^{46}\,\mathrm{erg\,s^{-1}}$ (K. Ichikawa et al. 2021, 2023). The inferred jet production efficiency calculated from $\eta_{\mathrm{jet}} \sim \epsilon_{\mathrm{rad}} P_{\mathrm{jet}}/L_{\mathrm{bol}}$ approaches unity, implying rapid spins of these nuclear BHs (e.g., A. Tchekhovskoy et al. 2011). These types of radio AGNs at intermediate redshifts may offer valuable insights into understanding the characteristics of LRDs at higher redshifts, thus further supporting our hypothesis of rapid BH spins.

4.5. Implications on BH Growth Mechanisms at $z \gtrsim 5$

The spin of a massive BH is influenced by a range of physical processes including BH mergers and mass accretion. The coalescence of two nonspinning BHs results in a remnant with a significant spin, approximately $a_\bullet \simeq 0.69$ for an equal-mass merger (E. Berti et al. 2007), but the spin diminishes if the merging BHs have nonzero, misaligned spins relative to the orbital angular momentum (e.g., E. Berti & M. Volonteri 2008).

Gas accreting onto BHs through a disk aligned with the angular momentum direction of the BH is expected to enhance the spin during mass accumulation (J. M. Bardeen et al. 1972; K. S. Thorne 1974). However, chaotic accretion characterized by short-lived episodes with random orientations tends to dampen the BH spin toward average values of $a_\bullet \simeq 0.2$ (e.g., A. R. King et al. 2008).

Chaotic accretion and related feeding mechanisms with low angular momentum gas are considered to promote the efficiency of BH mass growth in the early universe due to moderate centrifugal support (D. J. Eisenstein & A. Loeb 1995) and a lower radiative efficiency as a result of spin down (A. R. King et al. 2008). However, we show that the majority of the early BH populations growing in dust-rich environments tend to exhibit high spins with $a_\bullet \simeq 0.9$, corresponding to $\epsilon_{\mathrm{rad}} \gtrsim 0.2$. This suggests that BH growth is likely dominated by prolonged accretion episodes with coherent angular momentum, consistent with an idea pioneered by M. Volonteri et al. (2005), or a modest degree of anisotropy (M. Dotti et al. 2013; Y. Dubois et al. 2014). Cosmological simulations focused on galaxy assembly suggest that BHs retain high spins through coherent accretion modes. This occurs once BHs are settled down to the centers of their host galaxies, and then the BH spin direction is well aligned with the angular momentum of the hosts (S. Peirani et al. 2024). As a consequence, a significant fraction of AGNs are expected to launch radio jets and influence the BH–galaxy coevolution (e.g., R. S. Beckmann et al. 2024; see also Section 4.4).

Our conclusion regarding the rapid spins of BHs can be directly testable through future gravitational-wave observations with space-based detectors such as LISA (e.g., P. Amaro-Seoane et al. 2023). Moreover, if these BHs frequently merge during galaxy coalescences leading to the LRD phase or similar activities observed in ultraluminous infrared galaxies, such events could significantly contribute to a stochastic gravitational-wave background, detectable by pulsar-timing array experiments (K. Inayoshi et al. 2018; see also G. Agazie et al. 2023). Therefore, further exploration of the rapidly spinning, overmassive BHs in LRDs is needed in multiple aspects.

Acknowledgments

We greatly thank Luis C. Ho for emphasizing the significance of the Soltan–Paczyński argument and for dedicating time to an inspiring discussion during the spring festival holiday. We also thank Dale D. Kocevski for sharing their SED fit results for the two LRDs detected in X-rays, which are used in Figure 6. We also wish to thank Xiaoyang Chen, Anna-Christina Eilers, Joseph F. Hennawi, Haojie Hu, Kazumi Kashiyama, Vasily Kokorev, Masafusa Onoue, Elia Pizzati, and Yasushi Suto for the constructive discussions. K. Inayoshi acknowledges support from the National Natural Science Foundation of China (12073003, 12003003, 11721303, 11991052, 11950410493) and the China Manned Space Project (CMS-CSST-2021-A04 and CMS-CSST-2021-A06). This work is also supported by Japan Society for the Promotion of Science (JSPS) KAKENHI (20H01939; K. Ichikawa).

ORCID iDs

Kohei Inayoshi https://orcid.org/0000-0001-9840-4959
Kohei Ichikawa https://orcid.org/0000-0002-4377-903X

References

Agazie, G., Anumarlapudi, A., Archibald, A. M., et al. 2023, ApJL, 952, L37
Aird, J., Coil, A. L., Georgakakis, A., et al. 2015, MNRAS, 451, 1892
Akins, H. B., Casey, C. M., Lambrides, E., et al. 2024, arXiv:2406.10341
Amaro-Seoane, P., Andrews, J., Arca Sedda, M., et al. 2023, LRR, 26, 2
Ananna, T. T., Treister, E., Urry, C. M., et al. 2019, ApJ, 871, 240
Bardeen, J. M., Press, W. H., & Teukolsky, S. A. 1972, ApJ, 178, 347
Barro, G., Pérez-González, P. G., Kocevski, D. D., et al. 2024, ApJ, 963, 128
Beckmann, R. S., Smethurst, R. J., Simmons, B. D., et al. 2024, MNRAS, 527, 10867
Berti, E., Cardoso, V., Gonzalez, J. A., et al. 2007, PhRvD, 76, 064034
Berti, E., & Volonteri, M. 2008, ApJ, 684, 822
Blandford, R. D., & Znajek, R. L. 1977, MNRAS, 179, 433

Boylan-Kolchin, M. 2023, NatAs, 7, 731
Dai, L., & Fang, K. 2017, MNRAS, 469, 1354
Davies, F. B., Hennawi, J. F., & Eilers, A.-C. 2019, ApJL, 884, L19
Delvecchio, I., Gruppioni, C., Pozzi, F., et al. 2014, MNRAS, 439, 2736
Ding, X., Onoue, M., Silverman, J. D., et al. 2023, Natur, 621, 51
Dotti, M., Colpi, M., Pallini, S., Perego, A., & Volonteri, M. 2013, ApJ, 762, 68
Dubois, Y., Volonteri, M., & Silk, J. 2014, MNRAS, 440, 1590
Duras, F., Bongiorno, A., Ricci, F., et al. 2020, A&A, 636, A73
Eilers, A.-C., Mackenzie, R., Pizzati, E., et al. 2024, arXiv:2403.07986
Eisenstein, D. J., & Loeb, A. 1995, ApJ, 443, 11
Fujimoto, S., Brammer, G. B., Watson, D., et al. 2022, Natur, 604, 261
Furtak, L. J., Zitrin, A., Plat, A., et al. 2023, ApJ, 952, 142
Greene, J. E., & Ho, L. C. 2005, ApJ, 630, 122
Greene, J. E., Strader, J., & Ho, L. C. 2020, ARA&A, 58, 257
Greene, J. E., Labbe, I., Goulding, A. D., et al. 2024, ApJ, 964, 39
Harikane, Y., Ono, Y., Ouchi, M., et al. 2022, ApJS, 259, 20
Harikane, Y., Zhang, Y., Nakajima, K., et al. 2023, ApJ, 959, 39
Ho, L. C., Filippenko, A. V., & Sargent, W. L. 1995, ApJS, 98, 477
Hu, H., Inayoshi, K., Haiman, Z., et al. 2022, ApJ, 935, 140
Ichikawa, K., Yamashita, T., Merloni, A., et al. 2023, A&A, 672, A171
Ichikawa, K., Yamashita, T., Toba, Y., et al. 2021, ApJ, 921, 51
Inayoshi, K., Harikane, Y., Inoue, A. K., Li, W., & Ho, L. C. 2022a, ApJL, 938, L10
Inayoshi, K., Ichikawa, K., & Haiman, Z. 2018, ApJL, 863, L36
Inayoshi, K., Ichikawa, K., Ostriker, J. P., & Kuiper, R. 2019, MNRAS, 486, 5377
Inayoshi, K., Kashiyama, K., Li, W., et al. 2024, ApJ, 966, 164
Inayoshi, K., Kashiyama, K., Visbal, E., & Haiman, Z. 2016, MNRAS, 461, 2722
Inayoshi, K., Nakatani, R., Toyouchi, D., et al. 2022b, ApJ, 927, 237
Izumi, T., Matsuoka, Y., Fujimoto, S., et al. 2021, ApJ, 914, 36
Kerr, R. P. 1963, PhRvL, 11, 237
King, A. R., Pringle, J. E., & Hofmann, J. A. 2008, MNRAS, 385, 1621
Kocevski, D. D., Onoue, M., Inayoshi, K., et al. 2023, ApJL, 954, L4
Kocevski, D. D., Finkelstein, S. L., Barro, G., et al. 2024, arXiv:2404.03576
Kokorev, V., Fujimoto, S., Labbe, I., et al. 2023, ApJL, 957, L7
Kokorev, V., Caputi, K. I., Greene, J. E., et al. 2024, ApJ, 968, 38
Kormendy, J., & Ho, L. C. 2013, ARA&A, 51, 511
Kroupa, P. 2001, MNRAS, 322, 231
Kulier, A., Ostriker, J. P., Natarajan, P., Lackner, C. N., & Cen, R. 2015, ApJ, 799, 178
Labbe, I., Greene, J. E., Bezanson, R., et al. 2023, arXiv:2306.07320
Langeroodi, D., & Hjorth, J. 2023, ApJL, 957, L27
Leitherer, C., Schaerer, D., Goldader, J. D., et al. 1999, ApJS, 123, 3
Li, W., Inayoshi, K., Onoue, M., et al. 2024a, ApJ, 969, 69
Li, Z., Inayoshi, K., Chen, K., Ichikawa, K., & Ho, L. C. 2024b, arXiv:2407.10760
Lynden-Bell, D. 1969, Natur, 223, 690
Maiolino, R., Marconi, A., Salvati, M., et al. 2001, A&A, 365, 28
Maiolino, R., Risaliti, G., Signorini, M., et al. 2024, arXiv:2405.00504
Maiolino, R., Scholtz, J., Curtis-Lake, E., et al. 2023, arXiv:2308.01230
Matsuoka, Y., Onoue, M., Iwasawa, K., et al. 2023, ApJL, 949, L42
Matthee, J., Naidu, R. P., Brammer, G., et al. 2024, ApJ, 963, 129
McWilliams, S. T., Ostriker, J. P., & Pretorius, F. 2014, ApJ, 789, 156
Murase, K., Kimura, S. S., Zhang, B. T., Oikonomou, F., & Petropoulou, M. 2020, ApJ, 902, 108
Nandra, K., Laird, E. S., Aird, J. A., et al. 2015, ApJS, 220, 10
Nanni, R., Vignali, C., Gilli, R., Moretti, A., & Brandt, W. N. 2017, A&A, 603, A128
Niida, M., Nagao, T., Ikeda, H., et al. 2020, ApJ, 904, 89
Novikov, I. D., & Thorne, K. S. 1973, in Black Holes (Les Astres Occlus), ed. C. DeWitt (New York: Gordon and Breach), 343
Pacucci, F., Nguyen, B., Carniani, S., Maiolino, R., & Fan, X. 2023, ApJL, 957, L3
Peirani, S., Suto, Y., Beckmann, R. S., et al. 2024, A&A, 686, A233
Pérez-González, P. G., Barro, G., Rieke, G. H., et al. 2024, ApJ, 968, 4
Pizzati, E., Hennawi, J. F., Schaye, J., et al. 2024, arXiv:2403.12140
Planck Collaboration, Aghanim, N., Akrami, Y., et al. 2020, A&A, 641, A6
Pouliasis, E., Ruiz, A., Georgantopoulos, I., et al. 2024, A&A, 685, A97
Reines, A. E. 2022, NatAs, 6, 26
Sargent, W. L. W., & Filippenko, A. V. 1991, AJ, 102, 107
Schaerer, D., Contini, T., & Pindao, M. 1999, A&AS, 136, 35
Shakura, N. I., & Sunyaev, R. A. 1973, A&A, 24, 337
Shankar, F., Weinberg, D. H., & Miralda-Escudé, J. 2009, ApJ, 690, 20
Sotan, A. 1982, MNRAS, 200, 115
Steffen, A. T., Strateva, I., Brandt, W. N., et al. 2006, AJ, 131, 2826
Stone, M. A., Lyu, J., Rieke, G. H., Alberts, S., & Hainline, K. N. 2024, ApJ, 964, 90
Tchekhovskoy, A., Narayan, R., & McKinney, J. C. 2011, MNRAS, 418, L79
Thorne, K. S. 1974, ApJ, 191, 507
Torres-Orjuela, A., Huang, S.-J., Liang, Z.-C., et al. 2024, SCPMA, 67, 259511
Ueda, Y., Akiyama, M., Hasinger, G., Miyaji, T., & Watson, M. G. 2014, ApJ, 786, 104
Ueda, Y., Akiyama, M., Ohta, K., & Miyaji, T. 2003, ApJ, 598, 886
Vito, F., Brandt, W. N., Yang, G., et al. 2018, MNRAS, 473, 2378
Volonteri, M., Madau, P., Quataert, E., & Rees, M. J. 2005, ApJ, 620, 69
Williams, C. C., Alberts, S., Ji, Z., et al. 2024, ApJ, 968, 34
Yu, Q., & Tremaine, S. 2002, MNRAS, 335, 965
Yuan, F., & Narayan, R. 2014, ARA&A, 52, 529
Yue, M., Eilers, A.-C., Ananna, T. T., et al. 2024, arXiv:2404.13290